ARTICLE

# Electricity Storage With High Roundtrip Efficiency in a Reversible Solid Oxide Cell Stack

Li-zhen Gan[a], Kui Xie[b]*

*a. School of Mechanical and Automotive Engineering, Hefei University of Technology, Hefei 230009, China*

*b. Key Lab of Design & Assembly of Functional Nanostructure, Fujian Institute of Research on the Structure of Matter, Chinese Academy of Sciences, Fuzhou 350002, China*

(Dated: Received on October 10, 2015; Accepted on January 6, 2016)

We theoretically investigate the electricity storage/generation in a reversible solid oxide cell stack. The system heat is for the first time tentatively stored in a phase-change metal when the stack is operated to generate electricity in a fuel cell mode and then reused to store electricity in an electrolysis mode. The state of charge ($H_2$ frication in cathode) effectively enhances the open circuit voltages (OCVs) while the system gas pressure in electrodes also increases the OCVs. On the other hand, a higher system pressure facilitates the species diffusion in electrodes that therefore accordingly improve electrode polarizations. With the aid of recycled system heat, the roundtrip efficiency reaches as high as 92% for the repeated electricity storage and generation.

**Key words:** Reversible solid oxide cell, State of charge, Heat storage, Electricity storage, Electricity generation

## I. INTRODUCTION

In recent years, renewable energies have been attracting a great deal of interests because they have huge potentials to solve the energy and environmental issues [1, 2]. Reversible solid oxide cell (RSOC) is a device that can efficiently store renewable electricity in the form of chemical fuels through the solid oxide electrolysis cell (SOEC) process and reversibly generate electricity by the solid oxide fuel cell (SOFC) conversion process. SOFC has many advantages including high efficiency, long-term stability, fuel flexibility, low emissions, and low cost [3−5]. SOEC is the reverse mode of SOFC and inherits most SOFC advantages. RSOC can operate at higher temperatures with favourable kinetics for energy conversion in a large scale. RSOC combines the SOFC and SOEC and has been considered as an alternative energy storage system and/or a possible system for smart grid [6].

For a RSOC stack, the roundtrip efficiency has been considered as one of the key factors to evaluate the performance of electricity storage/generation in the reversible system. It has been widely accepted that a roundtrip efficiency with 80% is well adapted to the commercialization requirements. It has been reported that a roundtrip efficiency in the range of 70%−86% is achieved with LSGM-electrolyte cell stack at low current densities at 600−650 °C [7]. The system heat significantly changes the operation temperatures in the range of −50°C to 200 °C and thermal management is therefore extremely important in the roundtrip cycles. It should be noted that the thermal management is a complicated system engineering that can remarkably increase the roundtrip efficiencies. However, the reversible heat storage is still a challenge at 800−1000 °C though some thermal managements combining the electricity storage/generation with heating/cooling system.

Heat storage using phase-change metals with high heat capacity is an attractive option for high temperature thermal energy storage, especially at temperatures above 800 °C [8]. Under specific circumstances, the heat storage or release can be rapid, efficient and large-scale when a phase change material undergoes a phase transition from solid to solid, solid to liquid, or vice versa. It can store and release heat when being held constant at the phase transition temperature, and its reversible phase changing processes allow for repeated use. More importantly, the operation temperature can be easily extended to as high as 1000 °C to well adapt the operation temperature of solid oxide cell system. These advantages allow phase change metal tanks to be used as an advanced heat storage system for high temperature RSOC stacks. Copper or silver with high heat capacity, as common heat storage metals, can be readily intergraded into RSOC system to increase the roundtrip efficiencies.

In this work, a tubular RSOC stack combined with silver metal tank for heat storage is theoretically dem-

*Author to whom correspondence should be addressed. E-mail: kxie@fjirsm.ac.cn

 

onstrated. The charging and discharging processes have been modelled in relation to operation temperatures, system pressure, and state of charge. The roundtrip efficiency of electricity storage/generation is then studied.

## II. THE ELECTROCHEMICAL SIMULATION

### A. Open circuit voltage

The chemical reaction in RSOC is as follows:

$$\mathrm{H_2(g)} + \frac{1}{2}\mathrm{O_2(g)} \underset{\text{SOEC}}{\overset{\text{SOFC}}{\longleftrightarrow}} \mathrm{H_2O(g)}$$

which indicates the electricity generation/storage with $H_2/H_2O$ in fuel electrode and air in oxygen electrode. The open circuit voltage (OCV) hence can be calculated by the Nernst equation (Eq.(1) and Eq.(2)):

Fuel cell mode :

$$E_{\mathrm{OCV}} = E_0 - \frac{RT}{nF}\ln\left(\frac{p_{\mathrm{H_2O}}}{p_{\mathrm{H_2}}p_{\mathrm{O_2}}^{1/2}}\right) \tag{1}$$

Electrolysis cell mode :

$$E_{\mathrm{OCV}} = E_0 + \frac{RT}{nF}\ln\left(\frac{p_{\mathrm{H_2}}p_{\mathrm{O_2}}^{1/2}}{p_{\mathrm{H_2O}}}\right) \tag{2}$$

where $R$, $T$, $n$, and $F$ correspond to the universal gas constant (8.3145 J/(mol·K)), the system temperature in K, the number of electrons ($n$=2), and the Faraday constant (96485 C/mol), respectively. $p_{\mathrm{H_2O}}$, $p_{\mathrm{H_2}}$, and $p_{\mathrm{O_2}}$ are the partial pressures of steam, hydrogen, and oxygen, respectively. It can be seen that a higher stage of charge would be effective to increase the OCV values. The Gibb's free energy, for the reaction of $H_2$ and $O_2$ can be calculated via the relationship of $E^{\Theta}$ and enthalpy and entropy:

$$E^{\Theta} = \frac{\Delta G^{\Theta}}{nF} = -2.8976\times10^{-4}T + 1.2887 \tag{3}$$

### B. Ohmic resistance

The schematic of the reversible tubular fuel electrode-supported solid oxide cell is shown in Fig.S1 (supplementary materials) and the parameters of the components are shown in Table S1. The sequence flow of current through the interconnector, fuel electrode, electrolyte and the air electrode, and the current path of each component are clearly specified in Table S1 and S2 (supplementary materials). The resistance calculation for fuel electrode, air electrode, electrolyte, and interconnector, has been reported elsewhere [9]. The total ohmic resistance for RSOC is obtained by Eq.(4):

$$R_{\mathrm{ohmic}} = R_{\mathrm{fuel}} + R_{\mathrm{electrolyte}} + R_{\mathrm{oxygen}} + R_{\mathrm{interconnector}} \tag{4}$$

### C. Activation overpotential

The activation overpotential is the electrode surface overpotential and controlled by the kinetics at electrode surface. It is the external energy required to overcome the maximum activation energy barrier to maintain electrode reaction. The Butler-Volmer equations [10, 11] is used in the RSOC system. The activation polarization of the fuel electrode ($\eta_{\mathrm{act,f}}$) and that of air electrode ($\eta_{\mathrm{act,a}}$) can be expressed via mathematical transformation as indicated in Eq.(5) and (6):

$$\eta_{\mathrm{act,a}} = \frac{RT}{F}\ln\left[\frac{J}{2J_{0,\mathrm{a}}} + \sqrt{\left(\frac{J}{2J_{0,\mathrm{a}}}\right)^2 + 1}\right] \tag{5}$$

$$J_{0,\mathrm{f}} = \gamma_{\mathrm{f}}\frac{p_{\mathrm{H_2}}}{p}\frac{p_{\mathrm{H_2O}}}{p}\exp\left(-\frac{E_{\mathrm{act,f}}}{RT}\right) \tag{6}$$

$$\eta_{\mathrm{act,f}} = \frac{RT}{F}\ln\left[\frac{J}{2J_{0,\mathrm{f}}} + \sqrt{\left(\frac{J}{2J_{0,\mathrm{f}}}\right)^2 + 1}\right] \tag{7}$$

$$J_{0,\mathrm{a}} = \gamma_{\mathrm{a}}\left(\frac{p_{\mathrm{O_2}}}{p}\right)^{0.25}\exp\left(-\frac{E_{\mathrm{act,a}}}{RT}\right) \tag{8}$$

where $J$ is the current density, and $J_{0,\mathrm{a}}$ or $J_{0,\mathrm{f}}$ is a crucial parameter and depends on the electrode microstructure and operation conditions. The exchange current density can be calculated by Eq.(7) for the fuel electrode and Eq.(8) for the air electrode. The pre-exponential factors $\gamma_{\mathrm{f}}$ and $\gamma_{\mathrm{a}}$ are for fuel and air electrodes, respectively [12]. $E_{\mathrm{act,f}}$ and $E_{\mathrm{act,a}}$ are the activation energies of fuel electrode and air electrode, respectively. The $p_{\mathrm{O_2}}$ and $p_{\mathrm{H_2O}}$ is the partial pressure of gas $O_2$ and $H_2O$, $p$ is the total pressure.

### D. Concentration overpotential

In the reversible process, the concentration polarization simulations are performed both in fuel cell and electrolysis cell modes, respectively. In fuel cell mode, the concentration overpotentials of fuel electrode ($\eta_{\mathrm{conc,fuel,f}}$) and air electrode ($\eta_{\mathrm{conc,fuel,a}}$) can be calculated by Eq.(9) and Eq.(10), respectively [11, 12]:

$$\eta_{\mathrm{conc,fuel,f}} = \frac{RT}{2F}\ln\left[\frac{1 + \dfrac{RTl_{\mathrm{f}}J}{2FD_{\mathrm{H_2}}^{\mathrm{eff}}p_{\mathrm{H_2O}}}}{1 - \dfrac{RTl_{\mathrm{f}}J}{2FD_{\mathrm{H_2}}^{\mathrm{eff}}p_{\mathrm{H_2}}}}\right] \tag{9}$$

$$\eta_{\mathrm{conc,fuel,a}} = \frac{RT}{4F}\cdot \ln\left[p_{\mathrm{O_2}}\left(\frac{p_{\mathrm{a}}}{\delta_{\mathrm{O_2}}} - \left(\frac{p_{\mathrm{a}}}{\delta_{\mathrm{O_2}}} - p_{\mathrm{O_2}}\right)\exp\left(\frac{RTl_{\mathrm{a}}J\delta_{\mathrm{O_2}}}{4FD_{\mathrm{O_2}}^{\mathrm{eff}}p_{\mathrm{a}}}\right)\right)^{-1}\right] \tag{10}$$

Here, $l_{\mathrm{f}}$ and $l_{\mathrm{a}}$ stand for the thickness of fuel and air electrode, respectively, $p_{\mathrm{a}}$ is the gas pressure at the

DOI:10.1063/1674-0068/29/cjcp1510229 

air electrode. $D_{H_2}^{eff}$ and $D_{O_2}^{eff}$ are the effective diffusion coefficients for hydrogen and oxygen, respectively [13], while the related parameters are shown in Table S3 (supplementary materials). In the electrolysis cell mode, the concentration overpotentials of air ($\eta_{conc,elec.,a}$) and fuel electrodes ($\eta_{conc,elec.,f}$), can be calculated by Eq.(11) and Eq.(12), respectively [14, 15].

$$\eta_{conc,elec.,a} = \frac{RT}{4F} \ln \left[ \frac{\sqrt{P_{O_2}^2 + \left(\frac{JRT\mu l_a}{2FK_c}\right)}}{P_{O_2}} \right] \quad (11)$$

$$\eta_{conc,elec.,f} = -\frac{RT}{2F} \ln \left[ \frac{1 - \frac{RTl_f J}{2FD_{H_2O}^{eff} P_{H_2O}}}{1 + \frac{RTl_f J}{2FD_{H_2O}^{eff} P_{H_2}}} \right] \quad (12)$$

where $D_{H_2O}^{eff}$ is the effective diffusion coefficients of steam, $\mu$ is the dynamic viscosity of oxygen and the calculation can be referred with the related data displayed in Table S3 and S4 (supplementary materials) [16, 17].

### E. Cell voltage

The types of voltage loss in the RSOC are ohmic loss, activation and concentration polarizations. The ohmic loss for each component is calculated using the Ohm's law and then the voltage drop is given as:

$$\eta_{ohmic} = IR_{ohmic} \quad (13)$$

Once the ohmic overpotential is known, the cell voltages can be obtained by Eq.(14) for fuel cell mode and Eq.(15) for electrolysis cell mode:

$$V_{fuel} = E_{ocv} - \eta_{ohmic} - \eta_{act,fuel}^{fuel} - \eta_{act,air}^{fuel} - \eta_{conc,fuel}^{fuel} - \eta_{conc,air}^{fuel} \quad (14)$$

$$V_{elec.} = E_{ocv} + \eta_{ohmic} + \eta_{act,fuel}^{elec.} + \eta_{act,air}^{elec.} + \eta_{conc,fuel}^{elec.} + \eta_{conc,air}^{elec.} \quad (15)$$

### F. Heat simulation

In this section, the heat simulation was carried out to investigate the system balance. The heat mainly comes from the reaction losses by conduction when the cells work, which, therefore, changes the system temperatures. Using the mathematical method, the dependence of system temperature on time is calculated by Eq.(16) for fuel cell mode and Eq.(17) for electrolysis cell mode [18]:

$$\left[ m_{cell} Cp_{cell} + m_{heat} Cp_{heat} + \sum \left( N_{gas,m} Cp_{gas,m} \right) \right] dT = \left( q_r + q_{ohmic} - q_{loss} \right) dt \quad (16)$$

$$\left[ m_{cell} Cp_{cell} + m_{heat} Cp_{heat} + \sum \left( N_{gas,m} Cp_{gas,m} \right) \right] dT = \left( -q_r + q_{ohmic} - q_{loss} \right) dt \quad (17)$$

where $q_r$ is the electrochemical heat of the system heat, $q_{ohmic}$ is the heat from the ohmic resistance, $q_{loss}$ is the heat loss through the system. $m_{cell}$ is the mass of cell, and the total heat capacity of the cell is $Cp_{cell}$. In the model, the heat storage of the metal phase change is used, so $M_{heat}$ is the mass of metal and $Cp_{heat}$ is its heat capacity. The values are in Table S5 (supplementary materials). In this work, the RSOC system is assumed to be in an insulated box in which temperature is fairly constant,

$$q_l = A \frac{\lambda}{l} \left( T_i - T_o \right) \quad (18)$$

where $A$ is the surface area of the box in $m^2$, $\lambda$ is the thermal conductivity in W/(m·K), $l$ is the thickness of the box in m, and $T_i$ and $T_o$ are the temperatures of inside and the outside box, respectively.

The heat capacity of various gases, $C_{pi,m}$, in modelling system as a function of temperature can be calculated by Eq.(19), $i$ represents the various gases, and the related data are recorded in Table S6 (supplementary materials). In the RSOC system, the gas is assumed to be ideal:

$$C_{pi,m} = \sum_{j=0}^{6} \left[ b_j \left( \frac{T}{1000} \right)^j \right] \quad (19)$$

The heat storage, $\chi$, is the percentage of silver metal that has melted of the total metal in the heat storage. The procedures of heat absorption and release are similar and can be calculated as follows:

$$\chi = \int_0^t \left( \frac{q_r + q_{ohmic} - q_{loss}}{E_{heat}} \right) dt \quad (20)$$

When the change of metal phase begins, the $\chi$ changes, however, the temperature of the system remain constant. When the time equals 0, $\chi$ is 0%, when all the metal has melted, $\chi$ equals 100% and the temperature of system rises again. The $q_r$, $q_{ohmic}$, and $q_{loss}$ are the heat generation or loss from reaction, ohmic resistance and system heat loss, respectively. The $E_{heat}$ is the total energy stored by the metal phase change. On the contrary, when the system is in the electrolysis cell mode, the metal cools down so that the heat is released from it and absorbed by the electrolysis reaction.

$$E_{heat} = \frac{m_{heat}}{M_{metal}} H_{fusion,heat} \quad (21)$$

DOI:10.1063/1674-0068/29/cjcp1510229 

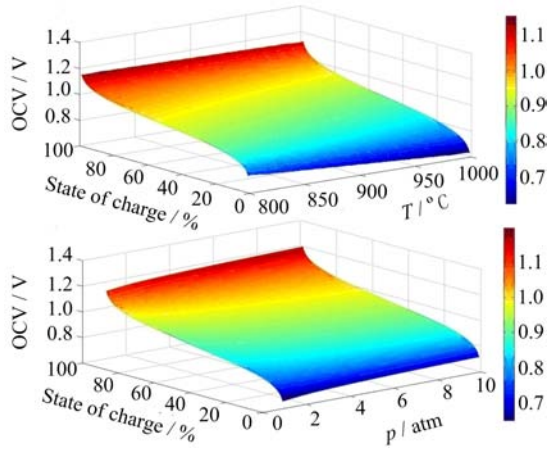


FIG. 1 The OCV of the RSOC system versus (a) temperature and (b) pressure in the state of charge (1%−99%).

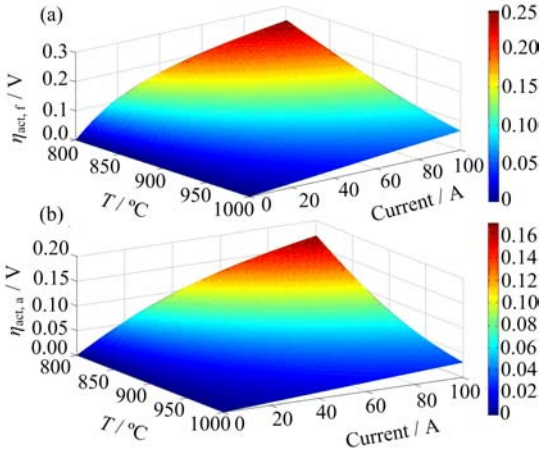


FIG. 2 Activation overpotentials in RSOC at 1 atm and 95% state of charge for the (a) fuel electrode and (b) air electrode, respectively.

Here, $M_{\text{metal}}$ is the molar mass of silver metal, and $E_{\text{heat}}$ is the total energy stored by the metal phase change. The $H_{\text{fusion,heat}}$ is the enthalpy of fusion for the metal.

## III. RESULTS AND DISCUSSION

Figure 1(a) shows the OCV of the RSOC system with the state of charge varying from 1% to 99% at different temperatures ranging from 800 °C to 1000 °C. The state of charge is defined as the mole fraction of hydrogen in the hydrogen/steam mixture at the fuel electrode in the system while the total operation pressure has always been considered as 1.0 atm. As anticipated, the OCV decreases at higher temperatures, which is consistent with results obtained in a previous work [19]. However, the OCV is significantly enhanced from 0.8 V to 1.1 V with the state of charge increases from 10% to 90% at 800 °C, as shown in Fig.1(b). Increasing operation pressure is expected to enhance the OCVs, however, the OCV only improves from 0.8 V to 0.85 V with system pressure increasing from 1 atm to 10 atm at the state of charge of 20% at 800 °C. The state of charge is an more important factor that affects the OCV and influences the RSOC system equilibrium.

Figure S3 shows the ohmic resistance of each component of a single RSOC cell. The main ohmic resistance is from the electrolyte, indicating the ionic transport limitation in reversible cells. Figure 2 illustrates the dependence of activation overpotential on both temperature and current for fuel electrode and air electrode, respectively. A remarkable increase in electrode overpotential is observed against current at 800 °C. This implies that a large current significantly increases the electrode overpotentials at lower temperatures. However, a linear relationship is observed between the overpotential and current at 1000 °C, which indicates that a higher current is favourable to improve electrode activation.

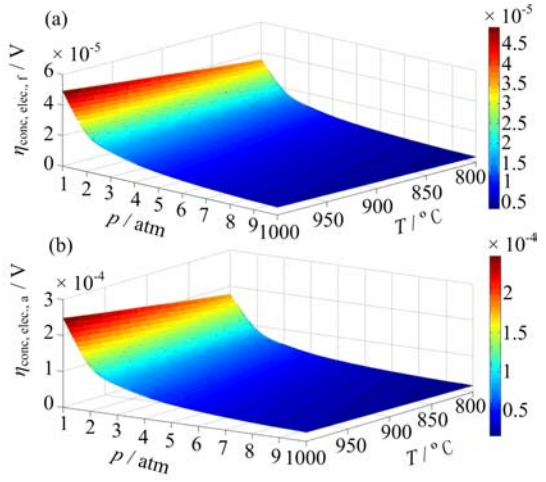


FIG. 3 Relationship between temperature, pressure and concentration overpotential in (a) fuel electrode and (b) air electrode at 1 A current and 95% state of charge in the fuel cell mode.

In addition, the fuel electrode polarization resistance is larger than that of air electrode. The optimization of fuel electrode to decrease polarization resistance would be therefore effective to enhance fuel electrode performance.

The pre-exponential factor is proportional to the length of triple phase boundary which can be determined by the size of grain, radius of pore, and porosity [20]. The influences of various pre-exponential factors on overpotentials is shown in Fig.S2 (supplementary materials). A porous electrode with sufficient triple phase boundary would be beneficial to electrode activity with lower pre-exponential factor. Figures 3 and 4 present the dependence of concentration overpotentials on pressures and temperatures in fuel cell mode and electrolysis mode, respectively. Although, the concentration overpotential is less dependent on temperature

DOI:10.1063/1674-0068/29/cjcp1510229 

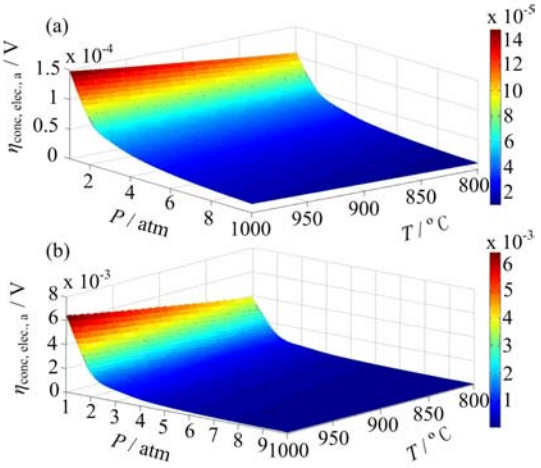


FIG. 4 Relationship between temperature, pressure and concentration overpotential in (a) fuel electrode and (b) air electrode at 1 A current and 95% state of charge in the electrolysis mode.

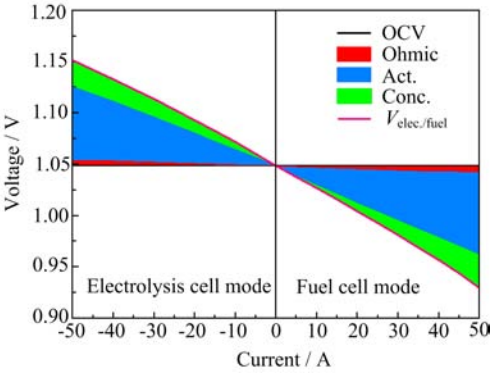


FIG. 5 Voltage of RSOC system versus current at 1 atm, 950 °C and with the state of charge 95%.

at higher pressure, it still improves at a higher temperature. The higher system pressure makes the concentration gradients smaller and not to be the main factor affecting concentration overpotentials. The concentration overpotential of fuel electrode in electrolysis cell mode is greater than that in fuel cell mode (see Fig.S3 and S4 in supplementary materials). This may be attributed to the larger Knudsen diffusion factor of hydrogen than that of steam under operation conditions. The currents also affect the concentration overpotentials of both electrodes either in fuel cell mode or electrolysis cell mode. The dependence of concentration overpotential on the currents and pressures in fuel cell and electrolysis cell mode at different temperature are also demonstrated in Fig.S5 and S6 (supplementary materials), respectively.

Figure 5 presents the *I-V* curves in the RSOC system, where the negative currents and the positive currents correspond to electrolysis cell mode and fuel cell mode, respectively. It is observed that the activation overpotential is the small primary source of voltage loss due to the thin electrodes. Apparently, the cell voltage losses from ohmic resistance is negligible owing to the low resistivity of materials and short current path. This means the improvement of electrode activity is the main challenge that restricts the cell performances.

In this work, a metal with phase change is utilized to store and reuse the heat generated in reversible system. The heat stored in phase-change metal in fuel cell mode and then reused in electrolysis mode strongly influences the energy storage capability of the RSOC system. The modelling assumed that the reversible system is located in an insulating box at current 1 A and total gas pressure 1 atm. The maximum temperature is set at 962 °C, in order to prevent the damage of the system. The temperature slowly increases as the heat generated from the chemical reaction. The generated heat competes with the heat loss in system and finally reaches an optimum at 962 °C after 838 s at which the fuel cell mode switches to electrolysis mode to avoid the overheat of the reversible system. The cooling procedure in electrolysis cell mode with 962 °C as the starting temperature. The temperature decreases to 800 °C after 731 s , and the electrolysis reaction stoped and switched back to fuel cell mode. The temperature change is demonstrated in Fig.S7 (supplementary materials), while the metal tank for heat storage is demonstrated in Fig.S8 (supplementary materials).

Figure 6 shows the state of charge, the heat storage percentage and temperature as a function of time in cycling process. The maximum temperature holds constant at 962 °C as the phase change of metal absorbs the generated heat. The state of charge decreases from 95% to 5% in fuel cell mode, and then the operation mode switches to electrolysis cell mode. The SOC could not reach 95% anymore because the heat loss is irreversible; however, it gets to 87.5%, which implies that the cycling efficiency is 92.1%. In fuel cell mode, the system temperature increases with the hydrogen consumption and reaches 962 °C, at which the metal begins to melt and absorbs the generated heat. Subsequently, the state of charge reduces to 5% at which the operation mode switched to electrolysis cell while 72.6% melted metal begins to release the absorbed heat to promote steam electrolysis. The system temperature returns to the initial state when the first cycle is completed with the exothermic steam electrolysis process terminated. The roundtrip efficiency for the first to the fifth cycle are 92.1%, 84.2%, 76.3%, 68.4%, and 60.5%, respectively. The recycle and utilization of exhaust heat is the advantage of solid oxide cells because of the high operation temperature. For example, coupling the solid oxide cell with heat sources like nuclear plants would be a useful way to recycle exhaust heat in addition to the heat storage in the system.

DOI:10.1063/1674-0068/29/cjcp1510229 

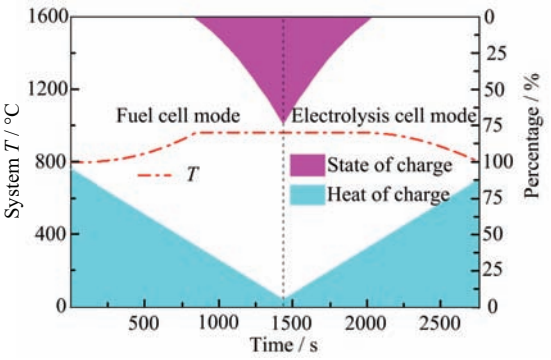


FIG. 6 Cycling performance of RSOC for the storage and utilization of electricity at 1 A per cell at the beginning conditions of 1 atm, 800 °C, and 95% state of charge.

## IV. CONCLUSION

In this work, a phase-change metal has been utilized to reversibly store and use system heat in an oxide conducting solid oxide electrolzyer. The electrochemical energy-conversion process has been modelled versus the operation conditions including temperature, pressure and state of charge. The roundtrip efficiency reaches as high as 92.1% for electricity storage and generation in the RSOC system. Other phase-change metal like copper can be utilized to store heat to enhance roundtrip efficiency while different melting point would affect the temperature equilibrium of solid oxide cell system. The RSOC system is an effective and efficient platform for the storage and generation of renewable electricity.

**Supplementary materials**: Tables S1, S2, S3, S4, S5, and S6 show the RSOC component parameters, input parameters, equation parameters, viscosity coefficients, heat simulation parameters and heat capacity coefficients, respectively. Figures S1, S2, S3, S4, S5, S6, S7, and S8 show the RSOC configuration, steam electrolysis energy balance, ohimic resistance of RSOC component, activation overpotential, concentration overpotential with pressure and temperature, concentration overpotential with pre-exponential factors, system temperature and phase-change metal tank configuration, respectively.

## V. ACKNOWLEDGMENTS

This work is supported by the National Natural Science Foundation of China (No.21303037 and No.91545123).

[1] K. Barnham, K. Knorr, and M. Mazzer, Nat. Mater. **11**, 908 (2012).
[2] G. Gahleitner, Int. J. Hydrogen. Energy **38**, 2039 (2013).
[3] S. Kakac, A. Pramuanjaroenkij, and X. Y. Zhou, Int. J. Hydrogen Energy **32**, 761 (2007).
[4] T. Papadam, G. Goula, and I. V. Yentekakis, Int. J. Hydrogen Energy **37**, 16680 (2012).
[5] M. Andersson, H. Paradis, J. L. Yuan, and B. Sunden, Int. J. Energ. Res. **35**, 1340 (2011).
[6] P. Aguiar, C. S. Adjiman, and N. P. Brandon, J. Power Sources **138**, 120 (2004).
[7] C. H. Wendel, Z. Gao, S. A. Barnett, and R. J. Braun, J. Power Sources **283**, 329 (2015).
[8] T. Nomura, C. Zhu, N. Sheng, G. Saito, and T. Akiyama, Sci. Rep. **5**, 9117 (2015).
[9] J. R. Ferguson, J. M. Fiard, and R. Herbin, J. Power Sources **58**, 109 (1996).
[10] S. Campanari and P. Iora, J. Power. Sources **132**, 113 (2004).
[11] S. H. Chan and Z. T. Xia, J. Appl. Electrochem. **32**, 339 (2002).
[12] M. Ni, M. K. H. Leung, and D. Y. C. Leung, Energ. Convers. Manage **48**, 1525 (2007).
[13] E. H. Pacheco, D. Singh, P. N. Hutton, N. Patel, and M. D. Mann, J. Power. Sources **138**, 174 (2004).
[14] M. Ni, M. K. H. Leung, and D. Y. C. Leung, Chem. Eng. Technol. **29**, 636 (2006).
[15] M. Ni, M. K. H. Leung, and D. Y. C. Leung, J. Power. Sources **163**, 460 (2006).
[16] B. Todd and J. B. Young, J. Power Sources **110**, 186 (2002).
[17] H. Y. Zhu, R. J. Kee, V. M. Janardhanan, O. Deutschmann, and D. G. Goodwin, J. Electrochem. Soc. **152**, A2427 (2005).
[18] K. Sedghisigarchi and A. Feliachi, IEEE. T. Energy. Conver **19**, 423 (2004).
[19] X. J. Chen, Q. L. Liu, S. H. Chan, N. P. Brandon, and K. A. Khor, Electrochem. Commun. **9**, 767 (2007).
[20] J. R. Ferguson, J. M. Fiard, and R. Herbin, J. Power Sources **58**, 109 (1996).

DOI:10.1063/1674-0068/29/cjcp1510229 